Two 3D Coordination Frameworks Based on Benzobisimidazole Linkers Generated under Similar Conditions: Synthesis, Structures and Thermal Properties

Shyam Biswas,*[a] Ying-Ya Liu,[b] Markus Tonigold,[c] Matthias Weil,[d] and Dirk Volkmer[e]

Herein, we present two benzobisimidazole-based 3D open coordination framework structures. Single-crystal X-ray analyses reveal that the title compounds $[Zn(H_2\text{-BBIM})(SO_4)]\cdot DMSO$ (**1**) (H_2-BBIM = benzobisimidazole; DMSO = dimethyl sulfoxide) and $[Co(H_2\text{-BBIM})(SO_4)(DMSO)_{0.5}]$ (**2**) possess two different framework structures, although both of them have been synthesized under similar conditions. Compounds **1** and **2** exhibit cubic diamondoid and tetragonal CrB_4 topological nets, respectively, in which the four-connected tetrahedral $\{MN_2O_2\}$ (M^{II} = Zn, Co) coordination units are located at the vertices and the edges are occupied by H_2-BBIM ligands and sulfate anions. Only tetracoordination is observed in **1**, whereas both tetra- and pentacoordination is present in **2**. The phase purity of the compounds was ascertained by X-ray powder diffraction (XRPD) analysis, infrared spectroscopy, and elemental analysis. Variable-temperature XRPD analysis indicated that **1** and **2** are stable up to 90 and 140 °C, respectively.

Introduction

Three-dimensional (3D) metal–organic polymers are of intense current interest because of their interesting physical properties, such as optical,[1] magnetic,[2] and electronic properties,[3] as well as their various possible applications in catalysis,[4] ion exchange,[5] gas storage,[6] separation,[7] sensing,[8] polymerization,[9] and drug delivery.[10] Given the wide variety of potential applications, successful synthetic strategies have been developed over the last few decades to meet the increasing global demand for this unique class of modular porous materials. By employing an isoreticular approach, the topological networks of some inorganic dense materials can be decorated or expanded[11] to modulate the framework pores and functionalize the pore walls. In general, rigid metal–organic coordination units, which are referred to as secondary building units (SBUs)[11a,11b,12] and have particular coordination configurations, are copolymerized with polytopic organic linkers with specific coordination modes in such a stereochemically predefined manner that the chemical and geometrical characteristics of both the SBUs and linkers are transferred to the resulting frameworks, which are effectively rigid and lack interpenetration.[13] The SBUs are judiciously selected from the existing database of discrete, low-molecular-weight coordination compounds. Basic metal carboxylates such as tri- and tetranuclear oxo-centered metal carboxylates, the latter of which serve as octahedral nodes, have been efficiently employed in the syntheses of well-known MIL-*n* (MIL = Matérial Institute Lavoisier)[14] and MOF-*n* (MOF = metal–organic framework)[11a,11b,15] families of isoreticular frameworks, respectively. Dinuclear paddlewheel carboxylates have also been used as square nodes for the construction of several MOF frameworks.[16] On the basis of their occurrence in the Cambridge Structural Database (CSD),[17] it has been proposed[11a,11b,18] and in fact observed that only a few tens of highly symmetric and regular nets ("default nets")[19] are expected to predominate over several hundreds of possible framework structures when a symmetric molecular building unit is assembled with a polydentate organic linker.

Porous zeolites are extensively used in petroleum cracking, ion exchange for water softening and purification, and separation of gases.[20] Zeolite structures are composed of tetrahedral $\{Si(Al)O_4\}$ units covalently connected by bridging O atoms to generate more than 150 different types of

[a] Indian Institute of Technology Guwahati, Department of Chemistry,
Guwahati, 781039 Assam, India
E-mail: sbiswas@iitg.ernet.in
http://www.iitg.ernet.in/sbiswas/
[b] State Key Laboratory of Fine Chemicals,
Dalian University of Technology,
116024, Dalian, China
[c] Current address: Clariant Produkte (Deutschland) GmbH,
Waldheimer Strasse 13, 83052 Bruckmuehl, Germany
[d] Institute for Chemical Technologies and Analytics, Division of Structural Chemistry, Vienna University of Technology,
Getreidemarkt 9/164-SC, 1060 Vienna, Austria
[e] Institute of Physics, Chair of Solid State Science, Augsburg University,
Universitätsstrasse 1, 86135 Augsburg, Germany

frameworks.[21] The incorporation of organic units such as imidazolates (IM) and transition-metal ions (especially tetracoordinate) into the zeolite frameworks has allowed us to expand their pore structures, enhance their functionality, and achieve new applications.[22] The resulting open frameworks with zeolite-like topologies (hence termed zeolitic imidazolate frameworks, or ZIFs)[23f,23h,23j,23k,23m] show many similarities with zeolites and can be used as porous materials for a variety of applications because of their exceptional thermal and chemical stability. The frameworks of most ZIF compounds bear tetrahedral $\{MN_4\}$ ("M" and "N" denote transition-metal atoms and N atoms of the imidazolate linkers, respectively) units at the vertices and the imidazolate ligands at the edges. The M (specifically Zn[23] or Co[23d,23f,23h,23j,23n,24]) atoms and the IM linkers have been purposely chosen to replace the T atoms (tetrahedral linkers such as Si, Al, and P) and the oxide bridges in zeolites, respectively, based on the fact that the M–IM–M angle is nearly 145° and that it is coincident with the Si–O–Si angle favored in many zeolites.

Most of the known MOFs have been synthesized using multidentate aryl-carboxylate ligands.[11,14–16] There are very few examples of MOFs that contain exclusively N-donor ligands such as 4,4′-bipyridines,[30] 1,2,3-triazolates,[31] 1,2,4-triazolates,[32] pyrazolates,[33] or tetrazolates.[34] The present study features the use of benzobisimidazole, which, to date, has rarely[35] been used to construct metal coordination polymers, although imidazole and its derivatives[23,24] have been extensively used to erect ZIF-type frameworks. In this article, we report on the syntheses, crystal structures, and thermal and spectroscopic properties of two benzobisimidazole-based Zn^{II} and Co^{II} coordination polymers.

Results and Discussion

Syntheses and Characterization

$[Zn(H_2\text{-BBIM})(SO_4)]\cdot DMSO$ (**1**) (H_2-BBIM = benzobisimidazole; DMSO = dimethyl sulfoxide) was initially obtained from the solvothermal reaction of $Zn(NO_3)_2\cdot 4H_2O$ and H_2-BBIM in DMSO (H_2-BBIM = benzobisimidazole; DMSO = dimethyl sulfoxide) at 120 °C for three days. Sulfate anions were generated in situ owing to the oxidation of DMSO by nitrate anions. Inspired by this observation, a more rational approach to synthesize **1** has been developed starting from the theoretical stoichiometric ratio (1:1) of H_2-BBIM and $ZnSO_4\cdot 7H_2O$ instead of $Zn(NO_3)_2\cdot 4H_2O$. However, the attempts to synthesize a putative isostructural Co^{II} compound using $CoSO_4\cdot 7H_2O$ by the solvothermal method under similar conditions (140 °C, 24 h) resulted in $[Co(H_2\text{-BBIM})(SO_4)(DMSO)_{0.5}]$ (**2**), which has a completely different framework topology compared to **1**. Both compounds are stable in air under ambient conditions. They are insoluble in water and common organic solvents including *N*,*N*′-dimethylformamide (DMF) and DMSO. The syntheses of **1** and **2** are summarized in Scheme 1.

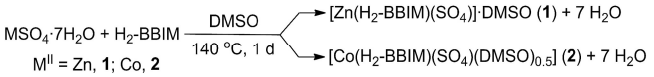

Scheme 1. Reaction scheme for the preparations of the two compounds demonstrated in this work.

The FTIR spectra of **1** and **2** (Figures S1 and S2 in the Supporting Information) display strong absorption bands at approximately 1120 cm^{-1}, which are attributed to the asymmetric stretching vibration (ν_3) of the coordinating sulfate anions.[36] The absorption bands for the S–O stretching vibration of DMSO molecules are probably overlapping with the ν_3 vibration of the sulfate anion in the region 1030–1120 cm^{-1}.[37]

The solid-state UV/Vis spectrum of **2** (Figure 1) exhibits two strong absorption bands due to the spin-allowed d–d transitions of tetrahedrally coordinated Co^{II} ions.[38] The relatively stronger absorption band at 580 nm is attributed to the transition from $^4A_{2g}$ to $^4T_{1g}$ (P) (ν_3), whereas the strong, broad absorption band in the region of 880–1100 nm is assigned to the transition from $^4A_{2g}$ to $^4T_{1g}$ (F) (ν_2). The absorption shoulder at 480 nm is indicative of the fact that the expectedly much weaker absorption bands of square-pyramidally coordinated Co^{II} ions are overlapped with the much stronger absorption bands of tetrahedrally coordinated Co^{II} ions.

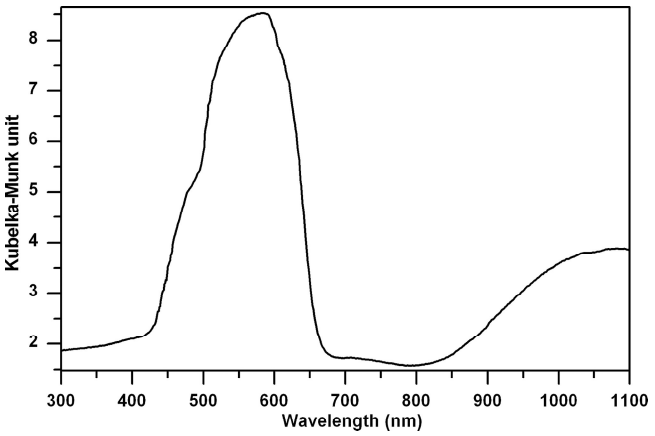

Figure 1. (a) UV/Vis diffuse reflectance spectrum of **2**.

Structural Description

As depicted in Scheme 2, the two coordination polymers **1** and **2** have been constructed using $\{MN_2O_2\}$ (M^{II} = Zn, Co; "N" and "O" represent the coordinating nitrogen and oxygen atoms of the H_2-BBIM ligands and sulfate anions, respectively) building units that resemble the tetrahedral units commonly found in zeolite frameworks. Although both of them are generated under similar solvothermal reaction conditions using DMSO as template, their crystal structures exhibit two different network types, each of which contains μ_2-benzobisimidazole and μ_2-sulfate bridges. Among the several edge-transitive[11b,19] nets with tetrahedral vertices, the cubic diamondoid (dia)[25] network of **1**

is the most regular and predominant,[26] and thus the default net for tetrahedral coordination. The structure of **2**, which is based on a tetragonal net often referred to as CrB_4[11c,27] (crb), the basis for the aluminosilicate framework in the monoclinic form of $CaAl_2Si_2O_8$,[28] is a non-default structure for tetrahedral building blocks and has rarely been[23f,23i,23j,24c,27a,29] observed in metal–organic and inorganic polymers. The formation of two different network types obtained by varying the metal(II) ions is attributed to the DMSO molecules (non-coordinating in **1**, but coordinating in **2**), which create different metal coordination environments (only tetracoordination in **1**, whereas both tetra- and pentacoordination exist in **2** in 1:1 proportions) and crystal-packing arrangements.

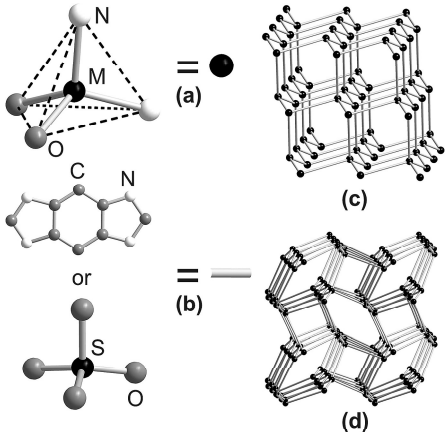

Scheme 2. Construction principles of the (c) diamondoid and (d) CrB_4 frameworks of **1** and **2**, respectively, comprising tetrahedral $\{MN_2O_2\}$ (M^{II} = Zn or Co) units (a), linked by (b) benzobisimidazole linkers and sulfate anions. Color codes are M, S: black; C, O: gray; N: white.

X-ray crystallographic analyses reveal that **1** crystallizes in the monoclinic space group $P2_1/n$, whereas **2** crystallizes in the orthorhombic space group $P2_12_12_1$. The crystal structures of **1** and **2** are shown in Figures 2 and 3, respectively.

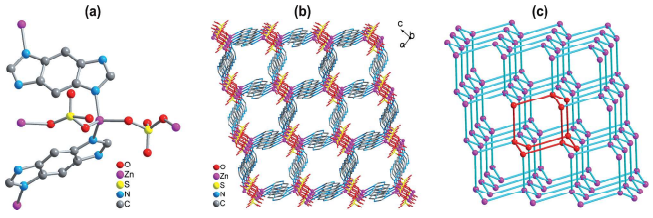

Figure 2. (a) Ball-and-stick representation showing the coordination environment around Zn^{II} ions in **1** (only the major part of the disordered SO_4 tetrahedron is shown). (b) Wire representation (except the Zn atoms, which are displayed as pink spheres) of the 3D framework of **1** viewed along the *b* axis. (c) Simplified representation of the 3D diamondoid topological net (point symbol: 6^6) of **1** obtained by replacing the H_2-BBIM ligands and sulfate anions with magenta sticks. The portion of the net (highlighted in red) represents the natural tiling of the diamondoid net. For clarity, hydrogen atoms and occluded DMSO molecules are omitted from all structural plots.

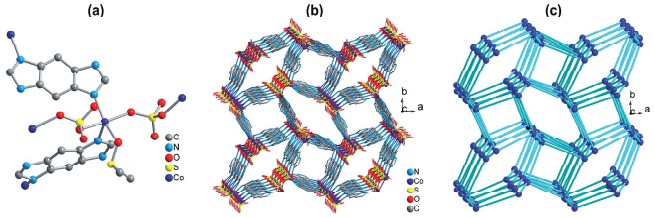

Figure 3. (a) Ball-and-stick representation displaying the square-pyramidal coordination environment around the Co^{II} ion in **2**. (b) Wire representation (except the Co atoms, which are displayed as blue spheres) of the 3D framework of **2** projected along the *c* axis; (c) Simplified representation of the CrB_4 net (point symbol: $4{\cdot}6^5$) of **2** obtained by replacing the H_2-BBIM ligands and sulfate anions with magenta sticks. Hydrogen atoms are omitted from all the structural drawings for clarity. For the same reason, the coordinating DMSO molecules that point towards the octagonal spindle-like cavities are also omitted from the plot (b).

The local coordination geometry around the Zn^{II} ions in **1** can be described as a distorted tetrahedron (Figure 2, a). Each Zn^{II} ion is coordinated by two different H_2-BBIM ligands through their N-donor atoms, and two dissimilar sulfate anions by means of their O-donor atoms. The O atoms of the crystallographically unique sulfate anion are disordered over two sets of sites in a 0.718(6):0.282(6) ratio. Similarly, each distorted-tetrahedral sulfate anion is coordinated by two Zn^{II} ions. Thus, each Zn^{II} ion is connected by four adjacent Zn^{II} ions through μ_2-benzobisimidazole and μ_2-sulfate bridges to result in a 3D polymeric framework structure (Figure 2, b). The 3D framework of **1** can be represented as a non-interpenetrating cubic diamondoid net (Figure 2, c) (with a point symbol of 6^6), in which the 4-connected, tetrahedral $\{ZnN_2O_2\}$ building units reside at the vertices, and the edges are occupied by both H_2-BBIM ligands and sulfate anions. The packing of **1** along the crystallographic *b* axis displays irregular edge-sharing hexagonal cavities. The smaller (5.50 Å) and the larger (8.59–8.92 Å) edges (i.e., intermetallic distances) of the hexagons are created owing to the cross-linking of the adjacent Zn^{II} ion by the sulfate anions and H_2-BBIM ligands, respectively. Void estimation with the PLATON program[39] using the single-crystal X-ray diffraction data of **1** reveals that the total potentially accessible void volume is 552 $Å^3$ if the guest DMSO molecules are not considered. This amounts to 36% of the unit-cell volume (1516.5 $Å^3$). Under ambient conditions, these void regions of the framework are filled with one ordered DMSO molecule per formula unit, in accordance with the thermogravimetric analysis (TGA) and elemental analysis. If the H_2-BBIM ligands and sulfate anions are not considered, the Zn–Zn–Zn angles in **1** range from 74.08 to 139.74° and deviate significantly from 109.45° expected for an idealized diamondoid network. The two types of Zn–N distances [1.975(4) and 1.997(4) Å] (Table 1) observed in **1** are in the range (1.98–2.08 Å) of distances reported previously for a huge variety of ZIFs that contain tetrahedrally coordinated Zn^{II} ions.[23]

It is worth mentioning that the linking of tetrahedral nodes with linear spacers is expected to generate one of the two equienergetic 3D nets, namely, cubic and hexagonal

Table 1. Selected bond lengths [Å] and angles [°] of **1**.[a]

Zn(1)–N(1)	1.997(4)	Zn(1)–O(1B)	2.001(10)
Zn(1)–N(3)	1.975(4)	Zn(1)–O(4A)#1	1.880(5)
Zn(1)–O(1A)	2.008(5)	Zn(1)–O(4B)#1	2.063(8)
N(3)–Zn(1)–N(1)	106.40(15)	O(1B)–Zn(1)–O(4A)#1	126.8(3)
N(3)–Zn(1)–O(1B)	89.1(3)	O(1A)–Zn(1)–O(4A)#1	84.0(3)
N(1)–Zn(1)–O(1B)	92.2(3)	N(3)–Zn(1)–O(4B)#1	107.3(3)
N(3)–Zn(1)–O(1A)	106.71(19)	N(1)–Zn(1)–O(4B)#1	99.5(3)
N(1)–Zn(1)–O(1A)	122.46(16)	O(1B)–Zn(1)–O(4B)#1	155.9(4)
N(3)–Zn(1)–O(4A)#1	118.58(17)	O(1A)–Zn(1)–O(4B)#1	113.5(3)
N(1)–Zn(1)–O(4A)#1	117.8(2)		

[a] Symmetry operator used to create equivalent atoms: #1: $-x + 1/2$, $y - 1/2$, $-z + 1/2$. A and B refer to the disordered parts of the sulfate tetrahedra.

diamondoid or lonsdaleite (lon) architectures. Metal coordination structures with hexagonal diamondoid topology are rare.[40] However, the cubic diamondoid topology is predominant with tetrahedral nodes. Since the pioneering work of Ermer et al. on hydrogen-bonded networks of adamantane-1,3,5,7-tetracarboxylic acid and methane tetraacetic acid,[41] a variety of compounds with interpenetrating and non-interpenetrating organic, metal–organic, and inorganic cubic diamondoid-like structures have been successfully prepared by connecting the tetrahedral nodes.[26]

Despite having a significant amount of pore volume as revealed from the void analysis, our repeated attempts to prove the permanent porosity of **1** have remained as yet unsuccessful. It was impossible to remove the solvent DMSO molecules completely from the pores of the as-synthesized samples of **1**, even after several solvent-exchange experiments (description of the guest-exchange studies are given in the Supporting Information) followed by heat treatment (at 323 K for 24 h under high vacuum). Moreover, the framework of **1** collapses after the exchange studies, as evident from the XRPD patterns (Figure S10 in the Supporting Information) of the corresponding samples. The destruction of the coordination network after removal of the guest molecules from its cavities has been previously observed in a wide variety of coordination frameworks that comprise single metal ions at the vertices and 4,4′-bipyridine at the links.[26a,42] The relative lack of directionality of a single Zn^{II} ion situated at the vertex of the net as well as the flexibility of the sulfate ions (which are less rigid than the H_2BBIM linkers) probably account for the structural collapse of the framework of **1**.

The structure of compound **2** adopts a completely different framework type than that of **1**. The network of **2** contains both tetra- and pentacoordinate Co^{II} ions, which are present in 1:1 proportions. The tetracoordinated Co^{II} ions reside in a distorted-tetrahedral environment; they are coordinated by two different H_2-BBIM ligands through their N-donor atoms and two distinct sulfate anions through their O-donor atoms. Therefore, the tetrahedrally coordinated metal(II) ions in both **1** and **2** have similar coordination geometries. The pentacoordinate Co^{II} ions in **2** are located in a square-pyramidal coordination environment (Figure 3, a) and are additionally connected by the O atom of a DMSO molecule. Each of the distorted sulfate anions is coordinated to a pair of Co^{II} ions. Analogous to the framework of **1**, each Co^{II} ion is connected with four neighboring Co^{II} ions through μ_2-benzobisimidazole and μ_2-sulfate bridges to result in a 3D polymeric network structure (Figure 3, b). The framework of **2** resembles the structure of the aluminosilicate $CaAl_2Si_2O_8$ with a CrB_4 topology (Figure 3, c) in which the 4-connected $\{CoN_2O_2\}$ nodes reside at the vertices, and the edges are occupied by both H_2-BBIM ligands and sulfate anions. If the coordinating DMSO molecules are not considered, an inspection of the framework along the crystallographic *c* axis reveals the presence of tetragonal and octagonal spindle-shaped cavities, with both of the resulting polygons being irregular. The DMSO molecules project towards the spindle-like cavities. Each of the octagons shares its smaller (5.56–5.66 Å) and larger (8.77–9.12 Å) edges with four other octagons and four tetragons, respectively. Similarly, every tetragon is connected by four octagons through the longer edges of the latter. The two pairs of opposite vertices of the octagons are connected in a twisted manner with the four vertices of the tetragons, thereby creating irregular edge-sharing boat-shaped hexagons between them. The 4-connected CrB_4 net of **2** has the point symbol (Figure S3 in the Supporting Information) of $4{\cdot}6^5$. Void estimation with the PLATON program[39] using the single-crystal X-ray diffraction data of **2** shows that the total potentially accessible void volume is 972 $Å^3$, which is 17% of the unit-cell volume (5744.0 $Å^3$). These values indicate that **2** possesses an almost nonporous framework, which is further confirmed by the N_2 sorption studies that exhibit no significant uptake of N_2 at 77 K by a heat-treated (at 373 K for 24 h under high vacuum) sample of **2**. The Co–N distances (Table 2) for the tetrahedrally

Table 2. Selected bond lengths [Å] and angles [°] of **2**.[a]

Co(1)–N(11)	2.088(10)	Co(3)–N(7)#2	1.953(11)
Co(1)–N(1)	2.104(9)	Co(3)–N(15)	1.955(10)
Co(1)–O(1)	2.039(7)	Co(3)–O(9)	1.916(9)
Co(1)–O(14)#1	2.046(7)	Co(3)–O(6)	1.982(7)
Co(1)–O(17)	2.087(8)	Co(4)–O(13)	1.922(8)
Co(2)–N(5)	2.063(9)	Co(4)–O(10)	1.959(7)
Co(2)–N(3)	2.089(11)	Co(4)–N(9)	2.003(9)
Co(2)–O(2)	2.058(8)	Co(4)–N(13)	2.011(11)
Co(2)–O(18)	2.058(8)		
Co(2)–O(5)	2.129(8)		
N(11)–Co(1)–N(1)	102.8(4)	O(2)–Co(2)–N(3)	95.9(4)
O(1)–Co(1)–O(14)#1	165.4(4)	O(2)–Co(2)–O(18)	90.1(3)
O(1)–Co(1)–O(17)	88.0(3)	O(2)–Co(2)–N(5)	86.1(4)
O(14)#1–Co(1)–O(17)	87.4(3)	O(18)–Co(2)–N(5)	162.8(4)
O(1)–Co(1)–N(11)	92.3(3)	O(18)–Co(2)–N(3)	96.3(4)
O(14)#1–Co(1)–N(11)	102.1(4)	O(2)–Co(2)–O(5)	168.7(3)
O(17)–Co(1)–N(11)	98.5(4)	O(18)–Co(2)–O(5)	86.2(3)
O(1)–Co(1)–N(1)	94.9(3)	N(5)–Co(2)–O(5)	94.3(3)
O(14)#1–Co(1)–N(1)	84.4(3)	N(3)–Co(2)–O(5)	95.1(3)
O(17)–Co(1)–N(1)	158.3(3)		
O(9)–Co(3)–N(7)#2	110.7(4)	O(13)–Co(4)–O(10)	109.7(4)
O(9)–Co(3)–N(15)	117.8(4)	O(13)–Co(4)–N(9)	111.3(4)
O(9)–Co(3)–O(6)	117.9(4)	O(10)–Co(4)–N(9)	117.6(4)
N(7)#2–Co(3)–O(6)	103.8(4)	O(13)–Co(4)–N(13)	99.4(4)
N(15)–Co(3)–O(6)	94.6(4)	O(10)–Co(4)–N(13)	108.7(4)

[a] Symmetry operators used to create equivalent atoms: #1: x, y, $z - 1$; #2: $x + 1/2$, $-y + 3/2$, $-z$.

and square-pyramidally coordinated Co^{II} ions in **2** are in the ranges of 1.95–2.01 and 2.06–2.10 Å, respectively. The average Co–N distance for the tetrahedrally coordinated (1.98 Å) Co^{II} ions, which is significantly shorter than that for the square-pyramidally coordinated (2.09 Å) Co^{II} ions, are in the range of distances (1.94–2.05 Å) documented previously for a large variety of ZIFs that bear tetrahedral Co^{II} ions.[23d,23f,23h,23j,23n,24]

TGA and XRPD

Phase purity of **1** and **2** was confirmed by elemental analysis and X-ray powder diffraction (XRPD) patterns recorded at ambient temperature. The experimental XRPD patterns (Figures S4 and S5 in the Supporting Information) are consistent with the simulated ones on the basis of the single-crystal X-ray diffraction data. Moreover, TGA and variable-temperature XRPD (VT-XRPD) experiments were performed to examine the thermal stability of both compounds. Compound **1** decomposes above 90 °C, whereas **2** possesses slightly higher thermal stability up to 140 °C.

In the TG curve of **1** (Figure 4, a), four mass loss steps are observed. The first mass loss is 10.9% from 90 to 270 °C, and the second step is 5.6% from 270 to 420 °C, both assigned to the loss of one non-coordinating DMSO molecule per formula unit (calcd. 19.6%). The framework collapses with the gradual liberation of occluded DMSO molecules from its cavities, as evidenced from the VT-

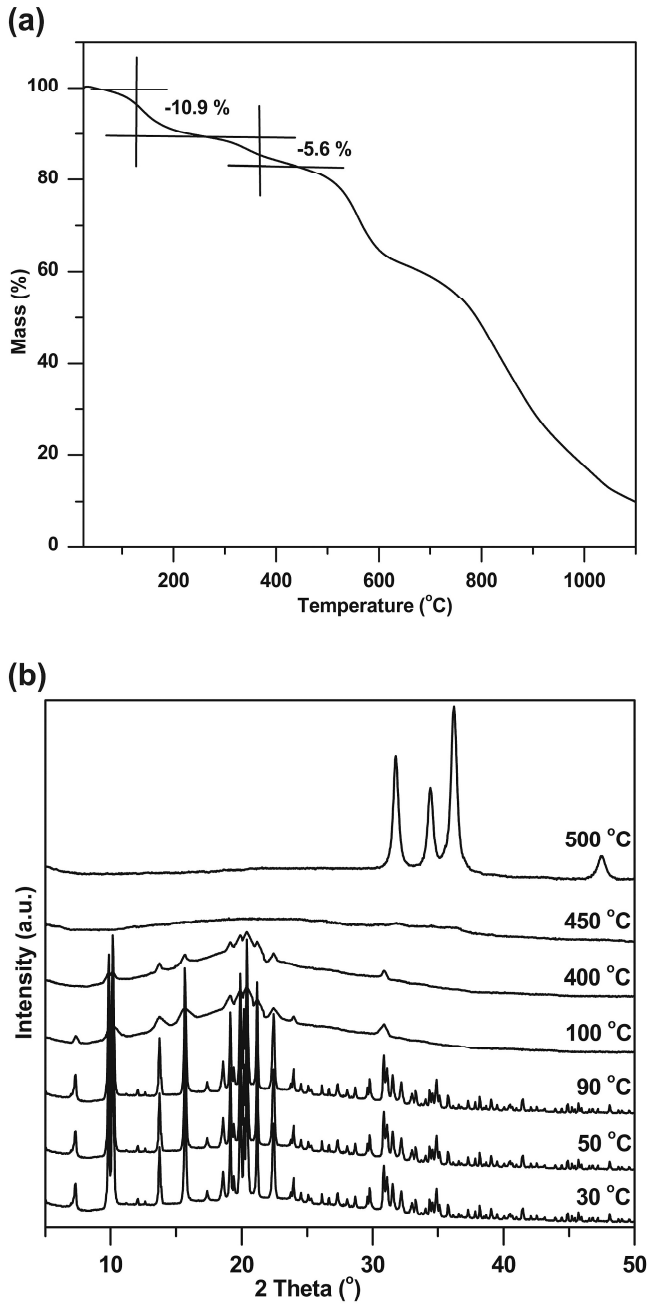

Figure 4. (a) Thermogravimetric analysis of **1** under nitrogen atmosphere. (b) VTXRPD plots of **1** in the range of 30–500 °C.

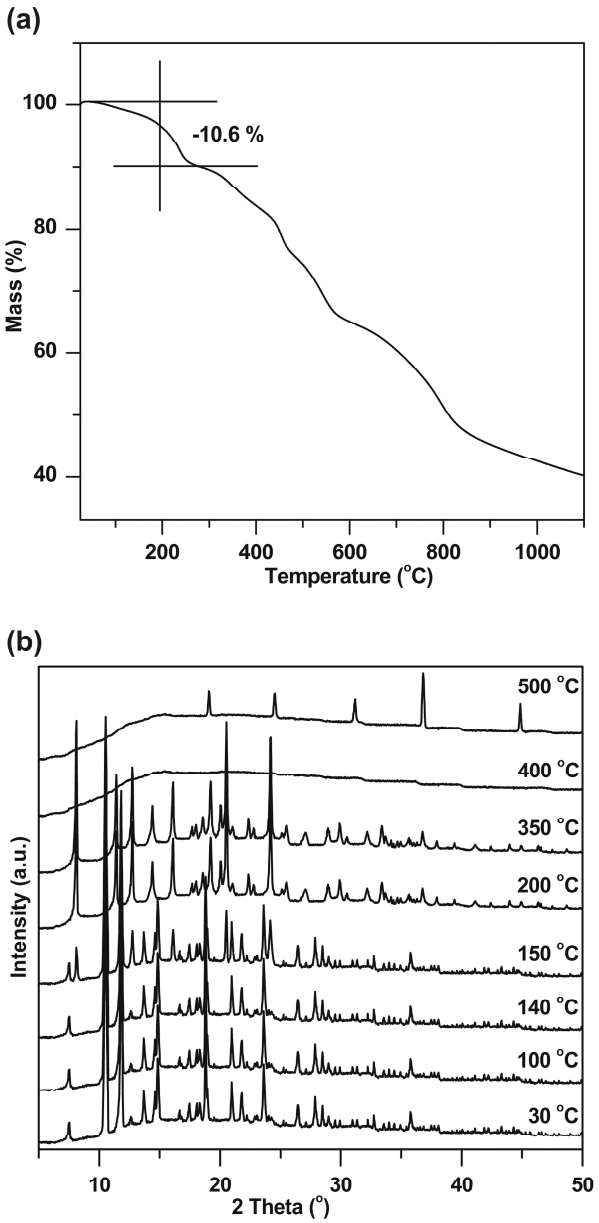

Figure 5. (a) Thermogravimetric analysis of **2** under nitrogen atmosphere. (b) VTXRPD plots of **2** in the range of 30–500 °C.

XRPD patterns (Figure 4, b). The third (22.1%) and fourth (51.5%) mass-loss steps are also due to the decomposition of this compound.

VT-XRPD studies (Figure 4, b) show that **1** is stable only up to 90 °C and crystallinity is lost upon the removal of free DMSO molecules. After that, the compound gradually loses its crystallinity and is completely amorphous at 450 °C. At 500 °C, ZnO appears as a new crystalline phase.

The TG trace of **2** (Figure 5, a) exhibits a five-step mass-loss process. The first mass loss of 10.6% in the temperature range 90–285 °C is attributed to the removal of 0.5 molecule of coordinating DMSO per formula unit (calcd. 11.1%). The second (6.4%), third (8.3%), fourth (10.5%), and fifth (24.4%) mass-loss steps are assigned to the decomposition of this compound.

From the VT-XRPD patterns (Figure 5, b), it becomes clear that **2** is stable up to 140 °C. At 150 °C, a new, unidentified crystalline phase appears along with the original phase of **2**. The new crystalline phase becomes predominant and retains its crystallinity in the temperature range 150–350 °C. This new phase loses its crystallinity completely at 400 °C and Co_3O_4 starts to appear at 500 °C.

Conclusion

We have prepared and fully characterized two compounds with different coordination framework structures (cubic diamondoid, **1**; tetragonal CrB_4, **2**), constructed from $\{MN_2O_2\}$ building units located at the vertices and μ_2-benzobisimidazole ligands and μ_2-sulfate anions situated at the edges. The formation of two different network types obtained by the variation of metal(II) ions under similar solvothermal reaction conditions in the same solvent (DMSO) demonstrates that the metal coordination geometry as well as the solvent (occluded or coordinating) used as template play crucial roles during the synthesis of crystalline phases of coordination polymers of similar composition. We believe that it will be possible to erect several other coordination framework structures by employing other first-row transition-metal ions. The existence of the two types of coordination environments (tetrahedral and square pyramidal) for the Co^{II} ions in **2** has been verified by electronic spectroscopy. IR spectra of both compounds are in accordance with coordinating sulfate anions based on the existence of their asymmetric stretching vibrations (ν_3). VT-XRPD experiments performed on **1** and **2** indicate that the frameworks are stable up to 90 and 140 °C, respectively. Although the present coordination polymers appear to be nonporous with low thermal stability, it might be feasible to construct truly porous frameworks that will be useful in gas storage and catalytic applications by using extended benzobisimidazole linkers. Moreover, the choice of amide solvents, which are known to deprotonate imidazole and its derivatives, might be helpful in designing ZIF-type materials that contain benzobisimidazole linkers.

Experimental Section

Materials and General Methods: The H_2-BBIM ligand was synthesized as described previously.[43] All starting materials were of reagent grade and used as received from commercial suppliers. FTIR spectra were recorded from KBr pellets in the range 4000–400 cm^{-1} with a Bruker IFS FTIR spectrometer. The following indications are used to characterize absorption bands: very strong (vs), strong (s), medium (m), weak (w), shoulder (sh), and broad (br). UV/Vis diffuse reflectance spectra (DRS) were recorded with an Analytik Jena Specord 50 UV/Vis spectrometer in the range of 300–1100 nm and converted into normal absorption spectra with the Kubelka–Munk function.[44] The lamps change wavelength at 320 nm, and the mirrors change at 370, 400, 700 and 900 nm. Elemental analyses (C, H, N) were carried out with a Perkin–Elmer 2400 elemental analyzer. TGA was performed with a TGA/SDTA851 Mettler Toledo analyzer in a temperature range of 25–1100 °C in flowing nitrogen at a heating rate of 10 °C min^{-1}. Ambient temperature X-ray powder diffraction (XRPD) patterns were measured with a Philips X′Pert PRO powder diffractometer operated at 40 kV, 40 mA for Cu target (λ = 1.5406 Å) with a scan speed of 30 s per step and a step size of 0.008°. Temperature-dependent X-ray powder diffraction measurements were performed in air with the same diffractometer equipped with an Anton Paar HTK 1200N reaction chamber. The heating rate between two temperatures was 5 °C min^{-1}, and once the corresponding temperature was reached, the sample was held at this temperature for 1 h before measuring the pattern. The simulated powder patterns were calculated on the basis of single-crystal X-ray diffraction data.

$[Zn(H_2\text{-BBIM})(SO_4)]\cdot$DMSO (1). Method A: A mixture of $ZnSO_4\cdot 7H_2O$ (18 mg, 0.06 mmol) and H_2-BBIM (10 mg, 0.06 mmol) was dissolved in DMSO (4 mL) and the solution was placed in a glass tube (10 mL). The tube was sealed and heated at 140 °C for 24 h, then cooled to room temperature. The supernatant was removed and the remaining colorless block-shaped crystals were successively washed with DMSO (3 × 1 mL) and methanol (3 × 2 mL), and dried in air to yield **1** (16 mg, 0.04 mmol, 64%). An X-ray diffraction study was performed on single crystals obtained from Method B. Crystals precipitated in both methods showed the same analytical results. $C_{10}H_{12}N_4O_5S_2Zn$ (397.74 mol^{-1}): C 30.19, H 3.04, N 14.08; found C 29.99, H 3.05, N 14.30. IR (KBr): $\tilde{\nu}$ = 3102 (br), 2913 (br), 2847 (w), 1723 (w), 1635 (m), 1511 (s), 1440 (m), 1377 (s), 1332 (w), 1270 (w), 1107 (vs), 1030 (vs), 968 (m), 954 (sh), 843 (m), 791 (w), 748 (w), 728 (w), 640 (w), 598 (s), 495 (w), 458 (m) cm^{-1}.

Method B: A mixture of $Zn(NO_3)_2\cdot 4H_2O$ (99 mg, 0.38 mmol) and H_2-BBIM (20 mg, 0.13 mmol) was dissolved in DMSO (4 mL) and the solution was placed in a glass tube (10 mL). The tube was sealed and heated at 120 °C for 72 h, then cooled to room temperature. The resulting colorless block-shaped crystals of **1** were collected by filtration, washed consecutively with DMSO (3 × 1 mL) and methanol (3 × 2 mL), and dried under vacuum to yield **1** (57 mg, 0.14 mmol, 38%).

$[Co(H_2\text{-BBIM})(SO_4)(DMSO)_{0.5}]$ (2): A mixture of $CoSO_4\cdot 7H_2O$ (18 mg, 0.06 mmol) and H_2-BBIM (10 mg, 0.06 mmol) was dissolved in DMSO (4 mL) and the solution was placed in a glass tube (10 mL). The tube was sealed and heated at 140 °C for 24 h, then cooled to room temperature. The supernatant was removed and the remaining purple block-shaped crystals were successively washed with DMSO (3 × 1 mL) and methanol (3 × 2 mL), and dried under vacuum to yield **2** (17 mg, 0.04 mmol, 68%). $C_9H_9CoN_4O_{4.5}S_{1.5}$ (352.22 g mol^{-1}): C 30.69, H 2.58, N 15.90; found C 30.45, H 2.53, N 15.89. IR (KBr): $\tilde{\nu}$ = 3098 (br), 2951

(br), 2843 (w), 1726 (w), 1655 (w), 1536 (sh), 1507 (s), 1412 (m), 1374 (s), 1267 (s), 1188 (sh), 1115 (vs), 1057 (m), 1027 (m) 946 (m), 845 (m), 795 (m), 627 (sh), 604 (s), 481 (m), 414 (w) cm^{-1}.

X-ray Crystallography: Structures of **1** and **2** were determined from single-crystal X-ray diffraction data. The intensity data of **1** were collected with a Bruker APEXII CCD diffractometer by employing monochromated Mo-K_α radiation (λ = 0.71073 Å) at T = 100 K. For **2**, the data were recorded with a STOE IPDS diffractometer using Mo-K_α radiation with graphite monochromatization (λ = 0.71073 Å) at T = 223 K. The structures of both compounds were solved by direct methods and refined by full-matrix least-squares techniques based on F^2 using the SHELXL-97 program.[45] Details of single-crystal data collection and refinement of **1** and **2** are summarized in Table 3. All structural plots were drawn using DIAMOND.[46]

Table 3. Single-crystal data and refinement summary for **1** and **2**.

	1	**2**
Formula	$C_{10}H_{12}N_4O_5S_2Zn$	$C_9H_9CoN_4O_{4.5}S_{1.5}$
M_r	397.74	352.22
T [K]	100(2)	223(2)
λ [Å]	0.71073	0.71073
Crystal dimensions [mm]	0.08 × 0.08 × 0.30	0.19 × 0.15 × 0.15
Crystal system	monoclinic	orthorhombic
Space group	$P2_1/n$	$P2_12_12_1$
a [Å]	11.318(3)	16.842(3)
b [Å]	9.601(3)	16.835(3)
c [Å]	13.965(4)	20.258(4)
α [°]	90.00	90.00
β [°]	92.063(14)	90.00
γ [°]	90.00	90.00
V [Å^3]	1516.4(7)	5743.9(18)
Z	4	16
$D_{calcd.}$ [g cm^{-3}]	1.742	1.629
μ [mm^{-1}]	1.922	1.432
$F(000)$	808	2848
θ range [°]	2.36–25.00	1.98–25.88
Measured reflections	17693	44799
Independent reflections	2662	11030
Data/restraints/parameters	2662/0/229	11030/438/722
R_1 [$I > 2\sigma(I)$][a]	0.0405	0.0640
wR_2 (all data)[b]	0.1033	0.1804
GoF on F^2	1.062	1.019
$\Delta\rho_{max./min.}$ [e Å^{-3}]	1.32/–0.99	1.41/–0.93

[a] $R1 = \Sigma||F_o| - |F_c||/\Sigma|F_o|$. [b] $wR_2 = \{\Sigma[w(F_o^2 - F_c^2)^2]/\Sigma[w(F_o^2)^2]\}^{1/2}$.

CCDC-1008224 (for **1**) and -1008225 (for **2**) contain the supplementary crystallographic data for this paper. These data can be obtained free of charge from The Cambridge Crystallographic Data Centre via www.ccdc.cam.ac.uk/data_request/cif.

Supporting Information (see footnote on the first page of this article): IR spectra, derivation of the point symbol for the network of **2**, XRPD patterns, optical micrographs, view of the asymmetric units, description of the solvent-exchange studies for **1**, and crystallographic information files (CIFs) for **1** and **2**.

Acknowledgments

S. B. is grateful to Indian Institute of Technology (IIT), Guwahati for a start-up research grant. D. V. acknowledges financial support from the German Research Foundation (DFG) (DFG Priority Program 1362 "Porous Metal–Organic Frameworks", VO 829/9-1). M. W. acknowledges the X-ray Centre of the Vienna University of Technology for the use of the single-crystal diffractometers.

[1] Y. Cui, Y. Yue, G. Qian, B. Chen, *Chem. Rev.* **2012**, *112*, 1126–1162.
[2] M. Kurmoo, *Chem. Soc. Rev.* **2009**, *38*, 1353–1379.
[3] a) W. Zhang, R.-G. Xiong, *Chem. Rev.* **2012**, *112*, 1163–1195; b) C. Wang, T. Zhang, W. Lin, *Chem. Rev.* **2012**, *112*, 1084–1104; c) C. G. Silva, A. Corma, H. García, *J. Mater. Chem.* **2010**, *20*, 3141–3156.
[4] J.-Y. Lee, O. K. Farha, J. Roberts, K. A. Scheidt, S.-B. T. Nguyen, J. T. Hupp, *Chem. Soc. Rev.* **2009**, *38*, 1450–1459.
[5] a) T. Y. Shvareva, S. Skanthakumar, L. Soderholm, A. Clearfield, T. E. Albrecht-Schmitt, *Chem. Mater.* **2007**, *19*, 132–134; b) D. F. Sava, V. C. Kravtsov, F. Nouar, L. Wojtas, J. F. Eubank, M. Eddaoudi, *J. Am. Chem. Soc.* **2008**, *130*, 3768–3770; c) Y. Liu, G. Li, X. Li, Y. Cui, *Angew. Chem. Int. Ed.* **2007**, *46*, 6301–6304; *Angew. Chem.* **2007**, *119*, 6417.
[6] a) S. Ma, H.-C. Zhou, *Chem. Commun.* **2010**, *46*, 44–53; b) M. P. Suh, H. J. Park, T. Kootteri Prasad, D.-W. Lim, *Chem. Rev.* **2012**, *112*, 782–835; c) K. Sumida, D. L. Rogow, J. A. Mason, T. M. McDonald, E. D. Bloch, Z. R. Herm, T.-H. Bae, J. R. Long, *Chem. Rev.* **2012**, *112*, 724–781.
[7] a) J.-R. Li, O. K. Farha, R. J. Kuppler, H.-C. Zhou, *Chem. Soc. Rev.* **2009**, *38*, 1477–1504; b) J.-R. Li, J. Sculley, H.-C. Zhou, *Chem. Rev.* **2012**, *112*, 869–932.
[8] L. E. Kreno, K. Leong, O. K. Farha, M. Allendorf, R. P. Van Duyne, J. T. Hupp, *Chem. Rev.* **2012**, *112*, 1105–1125.
[9] T. Uemura, N. Yanai, S. Kitagawa, *Chem. Soc. Rev.* **2009**, *38*, 1228–1236.
[10] P. Horcajada, T. Chalati, C. Serre, B. Gillet, C. Sebrie, T. Baati, J. F. Eubank, D. Heurtaux, P. Clayette, C. Kreuz, J. S. Chang, Y. K. Hwang, V. Marsaud, P.-N. Bories, L. Cynober, S. Gil, G. Férey, P. Couvreur, R. Gref, *Nat. Mater.* **2010**, *9*, 172–178.
[11] a) M. Eddaoudi, D. B. Moler, H. Li, B. L. Chen, T. M. Reineke, M. O'Keeffe, O. M. Yaghi, *Acc. Chem. Res.* **2001**, *34*, 319–330; b) O. M. Yaghi, M. O'Keeffe, N. W. Ockwig, H. K. Chae, M. Eddaoudi, J. Kim, *Nature* **2003**, *423*, 705–714; c) M. O'Keeffe, M. Eddaoudi, H. Li, T. Reineke, O. M. Yaghi, *J. Solid State Chem.* **2000**, *152*, 3–20.
[12] D. J. Tranchemontagne, J. L. Mendoza-Cortés, M. O'Keeffe, O. M. Yaghi, *Chem. Soc. Rev.* **2009**, *38*, 1257–1283.
[13] S. R. Batten, R. Robson, *Angew. Chem. Int. Ed.* **1998**, *37*, 1460–1494; *Angew. Chem.* **1998**, *110*, 1558.
[14] G. Férey, *Chem. Soc. Rev.* **2008**, *37*, 191–214.
[15] H. Furukawa, K. E. Cordova, M. O'Keeffe, O. M. Yaghi, *Science* **2013**, *341*, 974–986.
[16] M. Köberl, M. Cokoja, W. A. Herrmann, F. E. Kühn, *Dalton Trans.* **2011**, *40*, 6834–6859.
[17] F. H. Allen, *Acta Crystallogr., Sect. B* **2002**, *58*, 380–388.
[18] N. W. Ockwig, O. Delgado-Friedrichs, M. O'Keeffe, O. M. Yaghi, *Acc. Chem. Res.* **2005**, *38*, 176–182.
[19] O. Delgado-Friedrichs, M. O'Keeffe, O. M. Yaghi, *Phys. Chem. Chem. Phys.* **2007**, *9*, 1035–1043.
[20] a) T. L. M. Maesen, B. Marcus, in: *Introduction to Zeolite Science and Practice* (Eds.: H. van Bekkum, E. M. Flanigen, P. A. Jacobs, J. C. Jansen), Elsevier, Amsterdam, The Netherlands, **2001**, p. 1–9; b) D. W. Breck, in: *Zeolite Molecular Sieves*, Wiley, New York, **1974**.
[21] Ch. Baerlocher, L. B. McCusker, D. H. Olson, *Atlas of Zeolite Framework Types*, 6th rev. ed., Elsevier, Amsterdam, The Netherlands, **2007**; see also http://www.iza-structure.org/databases/.
[22] a) A. P. Wight, M. E. Davis, *Chem. Rev.* **2002**, *102*, 3589–3614; b) K. Yamamoto, Y. Sakata, Y. Nohara, Y. Takahashi, T. Tatsumi, *Science* **2003**, *300*, 470–472.
[23] a) C. I. H. Ashby, C. P. Chen, E. N. Duesler, T. L. Brown, *J. Am. Chem. Soc.* **1978**, *100*, 6063–6067; b) R. Lehnert, F. Seel, *Z. Anorg. Allg. Chem.* **1980**, *464*, 187–194; c) X. Huang, J. Zhang, X. Chen, *Chin. Sci. Bull.* **2003**, *48*, 1531–1534; d) Y.-Q. Tian, C.-X. Cai, X.-M. Ren, C.-Y. Duan, Y. Xu, S. Gao, X.-Z. You, *Chem. Eur. J.* **2003**, *9*, 5673–5685; e) H.-J. Xu, Y.-X. Liu,

Z. Shen, Y.-Q. Tian, X.-Z. You, *Z. Anorg. Allg. Chem.* **2005**, *631*, 1349–1351; f) K. S. Park, Z. Ni, A. P. Cote, J. Y. Choi, R. Huang, F. J. Uribe-Romo, H. K. Chae, M. O'Keeffe, O. M. Yaghi, *Proc. Natl. Acad. Sci. USA* **2006**, *103*, 10186–10191; g) X.-C. Huang, Y.-Y. Lin, J.-P. Zhang, X.-M. Chen, *Angew. Chem. Int. Ed.* **2006**, *45*, 1557–1559; *Angew. Chem.* **2006**, *118*, 1587; h) H. Hayashi, A. P. Cote, H. Furukawa, M. O'Keeffe, O. M. Yaghi, *Nat. Mater.* **2007**, *6*, 501–506; i) Y.-Q. Tian, Y.-M. Zhao, Z.-X. Chen, G.-N. Zhang, L.-H. Weng, D. Y. Zhao, *Chem. Eur. J.* **2007**, *13*, 4146–4154; j) R. Banerjee, A. Pahn, B. Wang, C. Knobler, H. Furukawa, M. O'Keeffe, O. M. Yaghi, *Science* **2008**, *319*, 939–943; k) B. Wang, A. P. Cote, H. Furukawa, M. O'Keeffe, O. M. Yaghi, *Nature* **2008**, *453*, 207–212; l) Q.-F. Yang, X.-B. Cui, X.-H. Yu, J. Lu, X.-Y. Yu, X. Zhang, J.-Q. Xu, Q. Hou, T.-G. Wang, *CrystEngComm* **2008**, *10*, 1534–1541; m) W. Morris, C. J. Doonan, H. Furukawa, R. Banerjee, O. M. Yaghi, *J. Am. Chem. Soc.* **2008**, *130*, 12626–12627; n) T. Wu, X. Bu, J. Zhang, P. Feng, *Chem. Mater.* **2008**, *20*, 7377–7382.

[24] a) M. Sturm, F. Brandl, D. Engel, W. Hoppe, *Acta Crystallogr., Sect. B* **1975**, *31*, 2369–2378; b) Y.-Q. Tian, C.-X. Cai, Y. Ji, X.-Z. You, S.-M. Peng, G.-H. Lee, *Angew. Chem. Int. Ed.* **2002**, *41*, 1384–1386; *Angew. Chem.* **2002**, *114*, 1442; c) Y.-Q. Tian, Z.-X. Chen, L.-H. Weng, H.-B. Guo, S. Gao, D. Y. Zhao, *Inorg. Chem.* **2004**, *43*, 4631–4635.

[25] For definitions of three-letter abbreviations, see the Reticular Chemistry Structure Resource (http://okeeffews1.la.asu.edu/RCSR/home.htm).

[26] a) M. J. Zawrotko, *Chem. Soc. Rev.* **1994**, *23*, 283–288; b) S. R. Batten, R. Robson, *Angew. Chem. Int. Ed.* **1998**, *37*, 1460–1494; *Angew. Chem.* **1998**, *110*, 1558; c) B. Moulton, M. J. Zawrotko, *Chem. Rev.* **2001**, *101*, 1629–1658.

[27] a) M. Schindler, F. C. Hawthorne, W. H. Baur, *Acta Crystallogr., Sect. B* **1999**, *55*, 811–829; b) M. O'Keeffe, B. G. Hyde, in: *Crystal Structures I: Patterns and Symmetry*, Mineralogical Society of America, Washington, DC, **1996**, ch. 7, p. 303–305. The CrB_4 net refers to the structure of the boron framework in that compound.

[28] Y. Takéuchi, N. Haga, J. Ito, *Z. Kristallogr.* **1973**, *137*, 380–398.

[29] a) C. Rong, Z. Yu, Q. Yang, S.-T. Zheng, C.-Y. Pan, F. Deng, G.-Y. Yang, *Inorg. Chem.* **2009**, *48*, 3650–3659; b) C.-Y. Pan, G.-Z. Liu, S.-T. Zheng, G.-Y. Yang, *Chem. Eur. J.* **2008**, *14*, 5057–5063; c) H. Li, A. Laine, M. O'Keeffe, O. M. Yaghi, *Science* **1999**, *283*, 1145–1147.

[30] X. Zhao, B. Xiao, A. J. Fletcher, K. M. Thomas, D. Bradshaw, M. J. Rosseinsky, *Science* **2004**, *306*, 1012–1015.

[31] a) S. Biswas, M. Grzywa, H. P. Nayek, S. Dehnen, S. Senkovska, S. Kaskel, D. Volkmer, *Dalton Trans.* **2009**, 6487–6495; b) X. L. Wang, C. Qin, S.-X. Wu, K.-Z. Shao, Y. Q. Lan, S. Wang, D. S. Zhu, Z.-M. Su, E.-B. Wang, *Angew. Chem. Int. Ed.* **2009**, *48*, 5291; *Angew. Chem.* **2009**, *121*, 5395.

[32] a) A. B. Lysenko, E. V. Govor, H. Krautscheid, K. V. Domasevitch, *Dalton Trans.* **2006**, 3772–3776; b) C. Yang, X. Wang, M. A. Omary, *J. Am. Chem. Soc.* **2007**, *129*, 15454–15455; c) W. Ouellette, M. H. Yu, C. J. O'Connor, D. Hagrman, J. Zubieta, *Angew. Chem. Int. Ed.* **2006**, *45*, 3497–3500; *Angew. Chem.* **2006**, *118*, 3577.

[33] a) H. J. Choi, M. Dincă, J. R. Long, *J. Am. Chem. Soc.* **2008**, *130*, 7848–7850; b) L. Hou, Y.-Y. Lin, X.-M. Chen, *Inorg. Chem.* **2008**, *47*, 1346–1351; c) M. Tonigold, Y. Lu, B. Brodenkötter, B. Rieger, S. Bahnmüller, J. Hitzbleck, G. Langstein, D. Volkmer, *Angew. Chem. Int. Ed.* **2009**, *48*, 7546–7550; *Angew. Chem.* **2009**, *121*, 7682.

[34] a) M. Dincă, A. F. Yu, J. R. Long, *J. Am. Chem. Soc.* **2006**, *128*, 8904–8913; b) M. Dincă, A. Dailly, Y. Liu, C. M. Brown, D. A. Neumann, J. R. Long, *J. Am. Chem. Soc.* **2006**, *128*, 16876–16883; c) M. Dincă, W. S. Han, Y. Liu, A. Dailly, C. M. Brown, J. R. Long, *Angew. Chem. Int. Ed.* **2007**, *46*, 1419–1422; *Angew. Chem.* **2007**, *119*, 1441.

[35] a) D.-D. Zhou, C.-T. He, P.-Q. Liao, W. Xue, W.-X. Zhang, H.-L. Zhou, J.-P. Zhang, X.-M. Chen, *Chem. Commun.* **2013**, *49*, 11728–11730; b) X. Yin, H. Chen, Y. Song, Y. Wang, Q. Li, L. Zhang, *J. Colloid Interface Sci.* **2014**, *413*, 175–182.

[36] a) C. R. Usher, C. A. Cleveland, D. R. Strongin, M. A. Schoonen, *Environ. Sci. Technol.* **2004**, *38*, 5604–5606; b) S. F. Maria, L. M. Russel, B. J. Turpin, R. J. Porcja, *Atmos. Environ.* **2002**, *36*, 5185–5196.

[37] a) K. Nakamoto, in: *Infrared and Raman Spectra of Inorganic and Coordination Compounds*, 4th ed., Wiley, New York, **1986**, p. 269–272; b) J. J. Rack, H. B. Gray, *Inorg. Chem.* **1999**, *38*, 2–3.

[38] A. B. P. Lever, *Inorganic Electronic Spectroscopy*, Elsevier, Amsterdam, **1968**, chapter 9, p. 299–305.

[39] A. L. Spek, *Acta Crystallogr., Sect. D* **2009**, *65*, 148–155.

[40] a) T. Kitazawa, T. Kikuyama, M. Takeda, T. Iwamoto, *J. Chem. Soc., Dalton Trans.* **1995**, 3715–3720; b) B. Sreenivasulu, J. J. Vittal, *Cryst. Growth Des.* **2003**, *3*, 635–637.

[41] a) O. Ermer, A. Eling, *Angew. Chem. Int. Ed. Engl.* **1988**, *27*, 829–833; *Angew. Chem.* **1988**, *100*, 856; b) O. Ermer, *J. Am. Chem. Soc.* **1988**, *110*, 3747–3754.

[42] A. J. Blake, N. R. Champness, P. Hubbertstey, W. Li, M. A. Withersby, M. Schröder, *Coord. Chem. Rev.* **1999**, *183*, 117–138.

[43] A. J. Boydston, K. A. Williams, C. W. Bielawski, *J. Am. Chem. Soc.* **2005**, *127*, 12496–12497.

[44] W. W. Wendlandt, H. G. Hecht, *Reflectance Spectroscopy*, Wiley-Interscience, New York, **1966**.

[45] G. M. Sheldrick, *Acta Crystallogr. Sect. A* **2008**, *64*, 112–122.

[46] K. Brandenburg, H. Putz, *DIAMOND*, version 3.0, *Crystal and Molecular Structure Visualization*, Crystal Impact GbR, Bonn, Germany.